A Full-Duplex Transceiver With Two-Stage Analog Cancellations for Multipath Self-Interference

Ying Liu, *Member, IEEE*, Patrick Roblin, *Senior Member, IEEE*, Xin Quan, *Student Member, IEEE*, Wensheng Pan, Shihai Shao, *Member, IEEE*, and Youxi Tang

***Abstract*— In this paper, a full-duplex transceiver with a two-stage analog interference cancellation architecture is proposed for the prevailing wireless full-duplex communication, which enables simultaneous transmission and reception on the same frequency. This two-stage cancellation architecture jointly combines the structures of two typical analog self-interference (SI) cancellation approaches, i.e., the radio frequency (RF)-tapping and the baseband-tapping approaches, and mitigates the SI signal in two steps to provide an improved analog cancellation performance with reduced restrictions on the RF components required to build the cancellation architecture. The stage-I cancellation uses a dual-tap analog canceling circuit to mitigate only the direct leakage and one refection component within the SI signal to yield a residual multipath SI of reduced dynamic range. In the stage-II cancellation, a nonlinear model is particularly designed to build a multipath canceling signal in digital domain, which is capable of characterizing the joint effect of the multipath SI propagation channel, the transmitter nonlinearity, and the receiver nonlinearity of high accuracy. The digital canceling signal is then transmitted through an auxiliary transmit chain to cancel the residual SI from the stage-I cancellation to further improve the overall analog cancellation performance. Simulations are explicitly performed on a variety of wideband signals to verify cancellation capability of the proposed full-duplex transceiver. For proof-of-concept verification, experiments are also performed on our self-designed testbed to validate the cancellation performances of each cancellation stage.**

***Index Terms*— Analog cancellation, full-duplex communication, multipath propagation channel, nonlinear distortion, self-interference (SI).**

I. Introduction

FULL-DUPLEX transceiver has gained much attention in both academia and industry for its capability of simultaneously transmitting and receiving on the same frequency carrier [1], [2] and the potential of doubling the throughput in theory [3]. Within a full-duplex transceiver, however, the transmitted signal also propagates into the local receiver through a direct path between the transmit and receive antennas [4] (or the direct leakage path of a single-antenna case [5]) and the reflection paths created by the transmit signal scattering off nearby objects, as demonstrated by the example shown in Fig. 1. These transmitted signals combine together at the RF front-end of the local receiver and become a self-interference (SI) that is overwhelmingly stronger than the desired signal from a remote user. For instance, a single-antenna full-duplex transceiver transmitting a signal of 20-MHz bandwidth at +20-dBm power level would generate an SI of up to 0 dBm, which is approximately 100 dB above the noise floor of the local receiver. This strong SI would saturate the analog-to-digital converter (ADC) of the receive chain, and thus needs to be suppressed at the RF front-end before the ADC quantization process [6], [7].

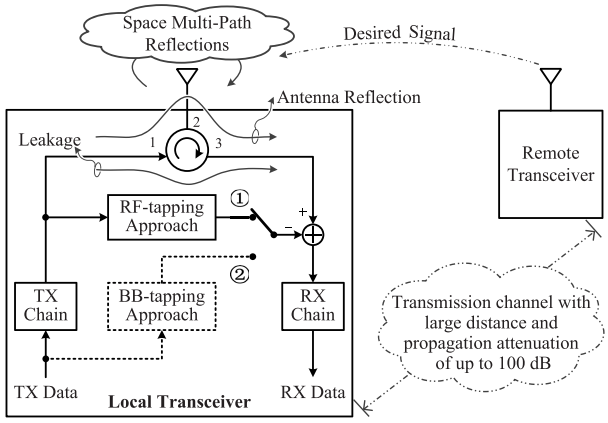

Fig. 1. Example of a single-antenna full-duplex transceiver with an analog cancellation using either: 1) the RF-tapping approach [4], [5] or 2) the BB-tapping approach [8].

Analog cancellation has been widely recognized as a necessary step to mitigate the SI, whose objective is to rebuild a copy of the RF SI waveform by some dedicated circuits. The rebuilt signal will be subsequently used to subtract from the received signal at the analog front-end of the local receiver to mitigate the strength of the SI signal. Generally, the analog cancellation techniques can be categorized into two major groups, i.e., the radio frequency (RF)-tapping approach and the baseband (BB)-tapping approach.

1) RF-Tapping Approach: The RF-tapping approaches [4], [5], [9], [10] are featured by using a dedicated circuit of some tunable RF components to reconstruct the SI signal from a coupled RF transmitted signal. For instance, the single-tap design

Manuscript received July 2, 2017; accepted September 10, 2017. Date of publication September 29, 2017; date of current version December 12, 2017. This work was supported in part by the National Natural Science Foundation of China under Grant 61701075, Grant 61771107, Grant 61771115, Grant 61531009, and Grant 61471108, in part by the National Major Projects under Project 2016ZX03001009, in part by Fundamental Research Funds for the Central Universities, and in part by the China Post-Doctoral Science Foundation. This paper is an expanded version from the 2017 International Microwave Conference, Honolulu, HI, USA, June 4–9, 2017. *(Corresponding author: Ying Liu.)*

Y. Liu, X. Quan, W. Pan, S. Shao, and Y. Tang are with the National Key Laboratory of Science and Technology on Communications, University of Electronic Science and Technology of China, Chengdu 611731, China (e-mail: 15881069748@139.com).

P. Roblin is with the Department of Electrical and Computer Engineering, The Ohio State University, Columbus, OH 43210 USA.

Color versions of one or more of the figures in this paper are available online at http://ieeexplore.ieee.org.

Digital Object Identifier 10.1109/TMTT.2017.2752167

in [4] first uses a balanced/unbalanced (balun) transformer to generate an inverted copy of the coupled RF transmitted signal in the analog domain and then uses a circuit to adjust the delay and attenuation of the inverted signal to match the SI at the receive antenna. However, due to the limited accuracy of practical programmable delays (with an achievable minimum resolution of 100 ps at the current stage), this approach can achieve only 25 dB in analog cancellation [10]. It has been shown that cancellation techniques using similar single-tap structure can operate only over narrow instantaneous bandwidth [11] and inherently cannot address reflection paths from the environment. To alleviate this problem, the multitap design in [5] passes the coupled RF transmitted signal through a more complicated circuit that consists of 16 parallel fixed lines of different delays and tunable attenuators to reconstruct the multipath SI signal. It is reported that this approach is capable of adapting to more complex environments and can provide an analog cancellation of 45 dB [5]. However, the associated RF cancellation circuit contains 16 finely designed coaxial lines and tunable attenuators, which dramatically increases the complexities in hardware design and requires sophisticated algorithms for attenuation tuning instead of more general gradient descent approaches [10].

2) BB-Tapping Approach: The BB-tapping approach [8] is featured by building a digital copy of the SI signal from the BB transmitted signal and then transmitting the digital copy through an auxiliary transmit chain (i.e., the canceling transmitter) to reconstruct the RF SI signal. In this approach, a finite impulse response (FIR) filter is implemented in the digital domain to characterize the SI propagation channel to generate a reconstructed SI signal of multipath components. The transmission delay and amplitude of the reconstructed SI signal can be easily adjusted by modifying the coefficients of the FIR filter to ensure that it is a close match of the practical SI signal [9], [12]. Besides, this approach can be easily extended to cover applications with more multipath components by simply increasing the order of the FIR filter. However, the disadvantages of this approach are also obvious. First, as the two transmit chains are not coherent with each other, the nonlinear distortion and the noise introduced by the main transmitter cannot be mitigated by canceling signal generated from the auxiliary transmitter. Second, due to the inherent noise of the transmitter circuit and the limited dynamic range of the digital-to-analog converter (DAC) in the canceling transmitter, the signal-to-noise ratio (SNR) of the canceling signal is limited. Therefore, although the strength of SI can be reduced by this analog cancellation approach to some extent, the associated impairments would become new sources of interference that significantly raise the noise floor of the local receiver [5].

In this paper, by exploiting the advantages of the two typical SI cancellation approaches, we propose a joint SI cancellation approach. In this approach, the SI signal is split into two parts of strong amplitudes and weak amplitudes, which are mitigated by two consecutive analog SI cancellation stages, respectively. In stage-I cancellation, a simple RF-tapping structure is adopted by deploying two identical canceling circuits for SI signal reconstruction. The first canceling circuit is used to reconstruct and counteract the direct leakage SI component, while the other one is used to track and suppress the antenna reflection for a full-duplex radio with single antenna or the strongest reflection from the varying environment for a full-duplex radio with separate antennas. With a simple gradient-based tuning algorithm, the dual-tap structure is capable of adapting to the varying environment as well as the temperature change of the RF components. In stage-II cancellation, a BB-tapping structure is adopted by including a novel nonlinear model, which characterizes the joint effect of the transceiver nonlinearity and SI multipath propagation, to provide a more accurate estimation and reconstruction of the multipath SI signal. Besides, as the dynamic range of stage-II cancellation is equivalently extended by an amount equal to the stage-I cancellation capability, the inherent noise of the auxiliary transmitter in this stage is reduced by the same amount. In summary, the two-stage cancellation is capable of mitigating both the strong components and the weak space multipath components of the SI signal, as well as the nonlinear distortion of the transceiver when transmitting at high power levels.

This paper is an extended version of [9] where the two-stage analog canceller was first introduced. This paper extends the work in [9] in three aspects.

1) The stage-I cancellation in [9] is extended to cover SI signal of wider bandwidth by including an extra cancellation circuit that is also capable of tracking and mitigating an extra strong reflection from either the antenna (for full-duplex radio with single antenna) or the varying environment (for full-duplex radio with separate antennas).
2) In stage-II cancellation, the channel model is extended from a simple linear FIR filter to a nonlinear model to characterize the joint effect of the multipath propagation channel, the transmitter nonlinear behavior, and the receiver nonlinear behavior. To the best of our knowledge, this is the first work addressing such an issue within a BB-tapping structure.
3) Along with the architecture description, a detailed introduction of the cancellation algorithms and exhaustive simulations and experimental results for SI cancellation performances are also presented in this paper.

This paper is organized as follows. In Section II, the signal model of the considered full-duplex transceiver with practical components is introduced. A detailed description of the proposed two-stage analog cancellation architecture and its tuning algorithms are presented in Section III. Measurement and simulation results are presented in Section IV. Conclusions are presented in Section V.

II. Full-Duplex Transceiver Model With Practical Components

The BB-equivalent structure of the analyzed full-duplex transceiver is illustrated in Fig. 2, which comprises a local transmitter, a local receiver, and a two-stage analog cancellation architecture. The transmitter first converts the BB signal $x[n]$ to its analog version $x(t)$, and then feeds it to the power amplifier (PA) for amplification before transmitting via

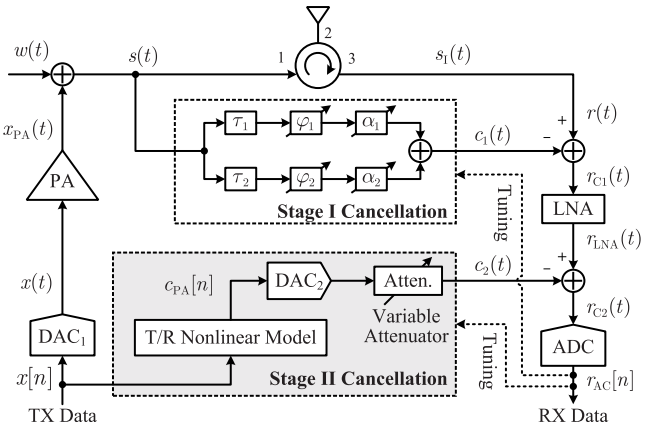

Fig. 2. Schematic of the BB-equivalent model of the analyzed full-duplex transceiver with the proposed two-stage analog cancellation.

the antenna. For typical wireless full-duplex communications, the transmitted $s(t)$ also propagates into the receive chain and becomes the SI signal $s_I(t)$. In this considered scenario, as the transmitter and the receiver share the same antenna by using a three-port circulator, the SI signal $s_I(t)$ (particularly, the direct leakage and the antenna reflection components) can be over 100 dB stronger than the desired signal from a remote user. Thus, it needs to be effectively mitigated; otherwise, it would saturate the ADC of the local receiver and prevent the desired signal from entering the receiver.

In this section, the principal behavioral model for each key component that contributes to the SI signal $s_I(t)$ is introduced, followed by a complete characterization for the SI waveform in different stages of the transceiver, taking into account the realistic multipath coupling channel, the transmitter nonlinearity, the receiver nonlinearity, and the transmitter noise.

A. SI Channel

The multipath channel impulse response between the transmit and the receive antennas can be given as

$$h(t) = \sum_{i=1}^{M} h_i \delta(t - \tau_i) \tag{1}$$

where h_i is the channel gain for the ith multipath component and $\delta\,(t-\tau_i)$ is the continuous-time unit impulse function (also known as delta function) with transmission delay τ_i. After propagation through the SI channel, the transmitted signal $s(t)$ becomes an SI signal $s_I(t)$ at the receiver RF front-end as

$$s_I(t) = s(t) \star h(t) = \sum_{i=1}^{M} h_i s(t - \tau_i) \tag{2}$$

where $(\star)$ denotes the convolution operation.

Note that (2) is also applicable to the single-antenna case, where $h_1\delta\,(t-\tau_1)$, $h_2\delta\,(t-\tau_2)$, and $\sum_{i=3}^{M} h_i\delta(t-\tau_i)$ represent the direct leakage path, the antenna reflection path, and the multipath reflection paths from the environment. Generally, for practical realization of small and low-cost full-duplex transceiver, the transmitter and receiver may use either the same antenna with a circulator or separate, but closely spaced antennas. In either case, the isolation between transmit and receive chains is limited, resulting in strong SI at the local receiver. Consider a single-antenna full-duplex transceiver using a 20-dB circulator isolation to connect the transmitter and the receiver. Transmitting a signal of 20-MHz bandwidth at +20 dBm will generate a leakage SI of 0 dBm power level at the local receiver RF front-end. This leakage SI is 97 dB above the receiver noise floor of −97 dBm with a 4-dB noise figure, and thus needs to be mitigated. Otherwise, it will saturate the receive chain and prevent the desired signal of a remote user from entering receiver.

B. Transmitter Nonlinearity

The strong nonlinearity of the PA and the relatively weak nonlinearities of the mixer and the DAC contribute to the overall transmitter nonlinearity [13], which can be approximated by a memory polynomial (MP) model [14], [15] as

$$x_{\mathrm{PA}}(t) = \sum_{k=0}^{K} \int_{0}^{t_Q} \gamma_{2k+1}(\tau)|x(t-\tau)|^{2k} x(t-\tau)d\tau \tag{3}$$

where

$$\gamma_k(t) = a_{kq}\delta(t-\tau_q), \quad q = 1, 2, \ldots, Q \tag{4}$$

$(2K+1)$ is the maximum order of nonlinearity, t_Q represents the maximum depth of memory effect, and a_{kq} is the complex coefficient of the MP model. For a PA with a typical third-order output intercept point (OIP3) of 35 dBm, the nonlinear distortion component is approximately 30 dB below the linear component when transmitting a 20-MHz signal at +20-dBm power level. After the 20-dB circulator isolation, the nonlinear distortion component at the receiver RF front-end would be 62 dB above the receiver noise floor of −97 dBm (with 20-MHz bandwidth and 4-dB noise figure).

C. Receiver Nonlinearity

The receiver nonlinearity is a combined effect of the relatively strong nonlinearity of the low-noise amplifier (LNA) and the weak nonlinearities of the mixer and the ADC of the receive chain [16]. For typical full-duplex applications, as the strength of the SI signal can be suppressed by the analog cancellations [4], [9] at the RF front-end, the residual SI that enters the receive chain would be much lower than the third-order input intercept point (IIP3) of the receive chain, more specifically, of the LNA. For example, for the case with the residual signal being 30 dB smaller than the IIP3 of the LNA, the nonlinear distortion components would be 60 dB lower than the SI signal. In such a case, the nonlinear distortion of the receiver would be much lower than that of the transmitter. However, as the transmission power increases, the nonlinear distortion of the receiver would become considerable. Thus, to model the weak nonlinearity of the receiver, a power series is used in this paper for simplicity

$$r_{\mathrm{LNA}}(t) = \sum_{k=0}^{K_R} b_k r_{C1}(t)|r_{C1}(t)|^{2k} \tag{5}$$

where $r_{\mathrm{LNA}}(t)$ and $r_{C1}(t)$ are the complex BB output and input of the LNA, respectively. $(2K_R+1)$ represents the maximum

order of nonlinearity of the receiver, which is typically less than the PA nonlinear order $(2K + 1)$. b_k is the complex coefficient of the LNA nonlinear model.

D. Transmitter Noises

Along with the PA nonlinear distortion, the transmitter also suffers from other imperfections, such as the phase noise of the local oscillator, the quantization noise of the DAC, and the inherent thermal noise of the transmitter circuit. From measurements in [17] and analysis in [18], the combined effects of these transmitter imperfections can be closely approximated by an independent zero-mean Gaussian noise $w(t)$, which is injected into the transmit chain after the PA as shown in Fig. 2. Thus, at the transmitter antenna port, the transmitted signal $s(t)$ is now given as

$$s(t) = x_{\mathrm{PA}}(t) + w(t) \tag{6}$$

with a typical SNR of approximately 60 dB for 20-MHz orthogonal frequency division multiplexed systems [5]. When the full-duplex transceiver transmits at +20-dBm power level, $w(t)$ would reach a power level of approximately −40 dBm, which is 37 dB (with 20-dB circulator isolation) above the receiver noise floor of −97 dBm. Thus, the transmitter noise should also be effectively suppressed; otherwise, it would become a new source of interference that would raise the noise floor and degrade the sensitivity of the local receiver.

In summary, the received SI signal at the RF front-end experiences the multipath propagation, the transmitter nonlinear distortion, and the receiver nonlinear distortion. In order to maximize the SI cancellation performance to reduce the stringent requirement on the dynamic range of the ADC, one needs to take these factors into consideration.

III. Proposed Two-Stage Analog Cancellation

As analog cancellation is critical to implement a full-duplex transceiver, simply applying conventional RF-tapping or BB-tapping approaches would raise stringent challenges on the RF components selection and tuning algorithm, yielding a limited SI cancellation performance. In this paper, by exploiting the advantages of the two approaches, a two-stage analog cancellation is proposed based on the signal model introduced in Section II.

A. Stage-I Analog Cancellation

The proposed stage-I analog cancellation uses a dual-tap structure as illustrated in the dashed box in Fig. 2. This structure can be regarded as an simple extension of the work in [9], where a one-tap structure was introduced for analog cancellation.

For a single-antenna case as shown in Fig. 2, the SI signal $s_I(t)$ in (2) is typically given by [19]

$$s_I(t) = \underbrace{h_1 s(t-\tau_1)}_{s_{IL}(t)} + \underbrace{h_2 s(t-\tau_2)}_{s_{IR}(t)} + \underbrace{\sum_{m=3}^{M} h_m s(t-\tau_m)}_{s_{IM}(t)} \tag{7}$$

which is a composite signal including three components: 1) the direct leakage $s_{IL}(t)$; 2) the antenna reflection $s_{IR}(t)$; and 3) the space multipath component $s_{IM}(t)$. As the direct leakage and antenna reflection components are much stronger than the space multipath components, the dynamic range of the composite SI signal $s_I(t)$ could be reduced by particularly mitigating $s_{IL}(t)$ and $s_{IR}(t)$ from $s_I(t)$, alienating the problem caused by the limited SNR of the auxiliary transmitter in BB-tapping approach.

This is similar for the case with separate antennas, where $s_{IL}(t)$, $s_{IR}(t)$, and $s_{IM}(t)$ represents the direct path, the strongest reflection, and the other weak reflections from the environment, respectively. In such a case, the proposed stage-I cancellation is also capable of tracking and mitigating one strong reflection from the environment, adding more flexibility and generality to the similar work in [9]. For simplicity, only the single-antenna case is considered and verified by simulations and experiments, in the following sections.

As illustrated in Fig. 2, analog canceller consists of two identical circuits, each of which contains a fixed delay d_i, a variable attenuator a_i, and a phase shifter ϕ_i with $i = 1$, 2, to counteract the direct leakage and the antenna reflection components introduced by the circulator. This analog canceller could provide some enhancement and flexibility compared with the one-tap designs [4], [9] with reduced complexity compared with the multitap designs [5]. As h_1, τ_1, h_2, and τ_2 are determined by the structure of the circulator, the antenna, and the feed line adopted, it is reasonable to consider them as invariable for any specific full-duplex radio. Consequently, this significantly reduces the complexity of the analog canceller by adjusting the attenuators and phase shifters using offline measurements and adapting them online within a smaller range.

To perform analog cancellation, a canceling signal $c_1(t)$ is generated by the analog canceller as

$$c_1(t) = \alpha_1 s(t-d_1)e^{j\phi_1} + \alpha_2 s(t-d_2)e^{j\phi_2}. \tag{8}$$

Four steps are carried out to ensure that $c_1(t)$ is an exact copy of the composite SI signal $(s_{IL}(t) + s_{IR}(t))$ with 180° phase shift, given the attenuators and phase shifters are finely calibrated.

1) Measure h_1, h_2, τ_1, and τ_2 using vector network analyzer.
2) Configure the two variable attenuators α_1 and α_2 with attenuations corresponding to h_1 and h_2, respectively.
3) Select appropriate transmission lines with $d_1 \approx \tau_1$ and $d_2 \approx \tau_2$.
4) Tune the phase shifters to ensure the power of the resulting signal after cancellation, i.e., $\mathbb{E}\{|r_{C1}(t)|^2\} = \mathbb{E}\{|r(t) - c_1(t)|^2\}$, reaches its minimum with $\phi_1 = (\tau_1 - d_1)/\omega_c + \pi$ and $\phi_2 = (\tau_2 - d_2)/\omega_c + \pi$, where ω_c is the carrier frequency.

After the four steps, the canceling signal $c_1(t)$ is generated as

$$c_1(t) = h_1 \frac{|s(t-d_1)|}{|s(t-\tau_1)|} s(t-\tau_1) + h_2 \frac{|s(t-d_2)|}{|s(t-\tau_2)|} s(t-\tau_2) \tag{9}$$

which closely approximates $(h_1\, s(t-\tau_1) + h_2\, s(t-\tau_2))$ given $|s(t-d_1)|/|s(t-\tau_1)| \approx 1$ and $|s(t-d_2)|/|s(t-\tau_2)| \approx 1$.

By subtracting $c_1(t)$ from the received SI signal $r(t)$ within the power combiner as shown in Fig. 2, the strength of the SI is reduced by an amount equal to the cancellation capability of this stage, which is defined as the power ratio between the SI signal before and after cancellations

$$G_{S1} = \frac{\mathbb{E}\{|r(t)|^2\}}{\mathbb{E}\{|r_{C1}(t)|^2\}} = \frac{\mathbb{E}\{|r(t)|^2\}}{\mathbb{E}\{|r(t) - c_1(t)|^2\}}. \tag{10}$$

As a result, the output of the power combiner $r_{C1}(t)$ mainly consists of the space multipath components and some parts of the leakage and antenna reflection, which can be expressed in a more general form as

$$r_{C1}(t) = \sum_{m=1}^{M} \tilde{h}_m s(t - \tau_m) \tag{11}$$

where $\tilde{h}_m$ $(m = 1, 2, \ldots, M)$ are the coefficients of the channel model for the residual multipath SI with $\tilde{h}_1 = h_1(1 - |s(t - d_1)|/|s(t - \tau_1)|)$, $\tilde{h}_2 = h_2(1 - |s(t - d_2)|/|s(t - \tau_2)|)$, and $\tilde{h}_m = h_m$ for $m = 3, 4, \ldots, M$.

It is shown in (11) that the residual SI signal $r_{C1}(t)$ is a superposition of M attenuated copies of the transmitted signal $s(t)$, with attenuation coefficients being $\tilde{h}_m$ $(M = 1, 2, \ldots, M)$. As the transmitter noise $w(t)$ is included within $s(t) = x_{\mathrm{PA}}(t) + w(t)$, it is naturally attenuated along with the SI signal by G_{S1}. If $\eta_{s1} + G_{S1} > G_{\mathrm{obj}}$ is satisfied where η_{s1} is the SNR of the transmitted signal $s(t)$ and G_{obj} is defined as the total cancellation amount required to suppress the SI close to the receiver noise floor, the transmitter noise $w(t)$ will drop below the receiver noise floor and will not impact the further SI cancellation that followed.

Note that the stage-I cancellation also alleviates the problem caused by the limited SNR of the auxiliary transmitter of the BB-tapping approach. The achieved cancellation capability G_{S1} equivalently extends the SNR of the BB-tapping approach by the same amount as G_{S1}. As such, the inherent transmitter noise of the auxiliary transmit chain would also drop below the receiver noise floor, if $\eta_{s2} + G_{S1} > G_{\mathrm{obj}}$ is satisfied, where η_{s2} is the SNR of the canceling signal $c_2(t)$ generated by the auxiliary transmitter.

Note that the leakage SI signal does not need to be completely canceled out at the current stage, and any residual leakage SI signal would be regarded as a component of the multipath SI $y_{\mathrm{MP}}(t)$ and could be further suppressed by the following multipath SI cancellation stage. Thus, this feature somehow relaxes the requirement on the accuracies of the RF devices used for phase and attenuation adjustments and it also reduces the complexity of the associated tuning algorithm.

B. Stage-II Analog Cancellation

After the stage-I SI cancellation, the dynamic range of the residual SI signal (composed of the space multipath SI signal and the residual leakage and antenna refection) is significantly reduced (by approximately G_{S1}), which also relaxes the dynamic range requirement on the DAC of the stage-II transmitter chain. However, for most full-duplex applications, the dynamic range of the residual multipath SI signal is still beyond that of the ADC ϵ_{ADC}, i.e., $G_{\mathrm{obj}} - G_{S1} > \epsilon_{\mathrm{ADC}}$. Thus, the objective of this analog cancellation stage is to mitigate the multipath components (space multipath reflections) of the SI to further suppress its strength.

The reconstruction of the canceling signal comprises three key steps: 1) digital multipath canceling signal modeling; 2) digital multipath signal generation; and 3) analog multipath canceling signal conversion. The major difference between this paper and the ones in [9] and [8] lies in the construction of the model used to characterize the multipath propagation channel between the transmit and receive antennas. In this paper, we use a nonlinear model to characterize the joint effect of the multipath channel, the transmitter nonlinearity, and the receiver nonlinearity, which is an extension from the linear FIR model used in [9].

1) Digital Multipath Canceling Signal Modeling: In this reconstruction stage, the digital transmitted signal $x[n]$ is used as the source signal to generate a digital version of the multipath SI signal that enters the receive chain. Thus, all the factors that contributes to the SI signal need to be considered, including the transmitter nonlinearity, the multipath SI channel, and the receiver nonlinearity.

For simplicity, the nonlinear order of the receiver model is chosen to be $K_{\mathrm{R}} = 3$, and thus, (5) is reduced to

$$r_{\mathrm{LNA}}(t) = b_1 r_{C1}(t) + b_1 r_{C1}(t)|r_{C1}(t)|^2 \tag{12}$$

where $r_{C1}(t)$ is the input of the LNA of the receiver. As $r_{C1}(t)$ can also be expressed as the analog residual SI model in (11), we could be closely approximate it by an FIR filter in the digital domain as [9]

$$r_{C1}[n] = \sum_{l=0}^{L-1} \hat{h}_l s[n - l] \tag{13}$$

in which $\hat{h}_l$ is the filter coefficient and L is chosen to ensure $L \times T_s \geq \tau_{M-1}$ satisfies, with T_s being the sampling time interval of the digitized signals $r_{C1}[n]$ and $s[n]$. Note that $\hat{h}_l$ attenuates the digital signal $s[n]$ by the same amount as $\tilde{h}_m$ does on the analog signal $s(t - \tau_m)$ in (11).

Thus, a digitized version for $r_{\mathrm{LNA}}(t)$ can be obtained

$$r_{\mathrm{LNA}}[n] = b_1 r_{C1}[n] + b_1 r_{C1}[n]|r_{C1}[n]|^2. \tag{14}$$

By substituting (13) into (14), we can obtain the joint model of the multipath channel and the receiver nonlinearity as

$$\begin{aligned} r_{\mathrm{LNA}}[n] &= \sum_{i=0}^{L-1} b_1 \hat{h}_l s[t - l] + \sum_{i=0}^{L-1} b_1 \hat{h}_l s[t - l] \left| \sum_{i=0}^{L-1} \hat{h}_l s[t - l] \right|^2 \\ &= \underbrace{\sum_{i=0}^{L-1} b_1 \hat{h}_l s[t - l]}_{r_{\mathrm{lin}}[n]} \\ &\quad + \underbrace{\sum_{q=0}^{L-1} \sum_{m=0}^{L-1} \sum_{l=0}^{L-1} b_3 \hat{h}_q \hat{h}_m \hat{h}_l s[t - q] s[t - m] s^*[t - l]}_{r_{\mathrm{non}}[n]} \end{aligned} \tag{15}$$

where $r_{\mathrm{lin}}[n]$ and $r_{\mathrm{non}}[n]$ are the linear model and third-order nonlinear model of the joint model.

By replacing the analog signals with their digitized versions in (3) and (6), we could relate the BB digital signal $x[n]$ with the transmitted signal $s[n]$ as

$$\begin{aligned} s[n] &= x_{\mathrm{PA}}[n] + w[n] \\ &= \sum_{k=0}^{K}\sum_{q=0}^{Q-1} a_{kq}x[n-q]|x[n-q]|^{2k} + w[n] \end{aligned} \tag{16}$$

where Q represents the maximum depth of memory effect. Thus, by substituting (16) into $r_{\mathrm{lin}}[n]$ in (15), we can obtain

$$\begin{aligned} r_{\mathrm{lin}}[n] &= \sum_{k=0}^{K}\sum_{q=0}^{Q-1}\sum_{l=0}^{L-1} \hat{h}_l a_{kq} x(n-q-l)|x(n-q-l)|^{2k} \\ &\quad + \sum_{l=0}^{L-1} \hat{h}_l w[n-l] \\ &= \sum_{k=0}^{K}\sum_{p=0}^{Q+L-1} \omega_{kp} x(n-p)|x(n-p)|^{2k} + \sum_{l=0}^{L-1} \hat{h}_l w[n-l] \end{aligned} \tag{17}$$

where

$$\omega_{kp} = \sum_{m=0}^{p} h_m a_{k(p-m)}, \quad (p \geq m) \tag{18}$$

is the coefficient for a regular MP nonlinear kernel with order $2k+1$ and memory p. It can be concluded from (17) that the L-tap multipath channel extends the memory depth of an MP model from Q to $(L+Q-1)$, yielding a new MP model with coefficients being ω_{kq}.

In order to obtain the digital model for the third-order distortion term $r_{\mathrm{non}}[n]$ within (15) in terms of the BB signal $x[n]$, we reform the transmitted signal $s[n]$ in (16) as

$$\begin{aligned} s[n] &= \underbrace{\sum_{q=0}^{Q-1} a_{0q}x[n-q]}_{s_{\mathrm{lin}}[n]} \\ &\quad + \underbrace{\sum_{k=1}^{K}\sum_{q=0}^{Q-1} a_{kq}x[n-q]|x[n-q]|^{2k}}_{s_{\mathrm{non}}[n]} + w[n] \end{aligned} \tag{19}$$

where $s_{\mathrm{lin}}[n]$ and $s_{\mathrm{non}}[n]$ represent the linear and the nonlinear components of the transmitted signal $s[n]$, respectively. For transmitter of high linearity, e.g., with the adjacent channel leakage ratio being below -45 dBc, the power of the nonlinear term $s_{\mathrm{non}}[n]$ is approximately 45 dB lower than that of the linear term $s_{\mathrm{lin}}[n]$ [24]. Feeding these two signal ($s_{\mathrm{lin}}[n] + s_{\mathrm{non}}[n]$) to the LNA, the nonlinear distortion caused by $s_{\mathrm{non}}[n]$ would be 125 dB smaller than that caused by $s_{\mathrm{non}}[n]$, and thus ignored for simplicity. As such, the third-order distortion term $r_{\mathrm{non}}[n]$ can now be closely approximated as

$$\begin{aligned} &r_{\mathrm{non}}[n] \\ &= \sum_{q=0}^{L-1}\sum_{m=0}^{L-1}\sum_{l=0}^{L-1} b_3 \hat{h}_q \hat{h}_m \hat{h}_l s[n-q]s[n-m]s^*[n-l] \\ &\approx \sum_{q=0}^{L-1}\sum_{m=0}^{L-1}\sum_{l=0}^{L-1} b_3 \hat{h}_q \hat{h}_m \hat{h}_l s_{\mathrm{lin}}[n-q]s_{\mathrm{lin}}[n-m]s^*_{\mathrm{lin}}[n-l] \\ &= \sum_{q=0}^{Q+L-1}\sum_{m=0}^{Q+L-1}\sum_{l=0}^{Q+L-1} \theta_{qml} x[n-q]x[n-m]x^*[n-l] \end{aligned} \tag{20}$$

where θ_{qml} is the model coefficient for third-order nonlinear kernel $x[n-q]x[n-m]x^*[n-l]$ given by

$$\theta_{qml} = b_3 \left(\sum_{i=0}^{q} \hat{h}_i a_{0i}\right)\left(\sum_{i=0}^{m} \hat{h}_j a_{0j}\right)\left(\sum_{i=0}^{l} \hat{h}_u a_{0u}\right). \tag{21}$$

Therefore, based on (16), (18), and (19), the signal model that combines the transmitter nonlinearity, the multipath SI channel, and the receiver nonlinearity is now given as

$$\begin{aligned} &r_{\mathrm{LNA}}[n] \\ &= \sum_{k=0}^{K}\sum_{p=0}^{Q+L-1} \omega_{kq} x[n-p]|x[n-p]|^{2k} \\ &\quad + \sum_{q=0}^{Q+L-1}\sum_{m=0}^{Q+L-1}\sum_{l=0}^{Q+L-1} \theta_{qml} x[n-q]x[n-m]x^*[n-l]. \end{aligned} \tag{22}$$

For typical indoor channel [20] with a maximum transmission delay of 400 ns, an FIR filter of $L = 40$ orders will be used to reconstruct the multipath channel (sampling rate being 100 MS/s), resulting in large number of coefficients for model (22). However, for many cases, we do not need all of the coefficients in practice. For instance, in some scenarios, depending on the signal bandwidth and sampling rate, it may not be necessary to implement all delay taps (p, q, m, and l). Therefore, in general, it is useful to rewrite (22) in terms of index arrays

$$\begin{aligned} r_{\mathrm{LNA}}[n] &= \sum_{k\in\mathcal{K}}\sum_{p\in\mathcal{P}} \omega_{kq} x[n-p]|x[n-p]|^{2k} \\ &\quad + \sum_{q\in\mathcal{Q}}\sum_{m\in\mathcal{M}}\sum_{l\in\mathcal{L}} \theta_{qml} x[n-q]x[n-m]x^*[n-l] \end{aligned} \tag{23}$$

where $\mathcal{K}$ is the index array selected from the PA nonlinear order array $\{0, 1, \ldots, K-1\}$, while $\mathcal{P}$, $\mathcal{Q}$, $\mathcal{M}$, and $\mathcal{L}$ are the index arrays selected from the transmission delay array $\{0, 1, \ldots, Q+L-1\}$.

2) Digital Multipath Canceling Signal Reconstruction: By considering the fact that the SI channel between the transmit and the receive chains remains constant within each transmit symbol, (23) could be written in a matrix form by gathering N samples within each transmit symbol as

$$\mathbf{r}_{\mathrm{LNA}} = \mathbf{\Omega X} \tag{24}$$

where

$$\mathbf{r}_{\mathrm{LNA}} = [r_{\mathrm{LNA}}(0), r_{\mathrm{LNA}}(1), \ldots, r_{\mathrm{LNA}}(N-1)]^T$$
$$\mathbf{\Omega} = [\mathbf{W}, \mathbf{\Theta}], \quad \mathbf{X} = [\mathbf{X}_1, \mathbf{X}_2].$$

Matrices $\mathbf{W}$, $\mathbf{\Theta}$, $\mathbf{X}_1$, and $\mathbf{X}_2$ are, respectively, defined as

$$\mathbf{W} = [w_{00}, \ldots, w_{kq}, \ldots, w_{K,(Q-1)}]$$
$$\mathbf{\Theta} = [\theta_{000}, \ldots, \theta_{qml}, \ldots, \theta_{(Q+L-1),(Q+L-1),(Q+L-1)}]$$
$$\mathbf{X_1} = [\mathbf{X}_0, \mathbf{X}_1, \mathbf{X}_2, \ldots, \mathbf{X}_{N-1}]^T$$
$$\mathbf{X_2} = [\tilde{\mathbf{X}}_0, \tilde{\mathbf{X}}_1, \tilde{\mathbf{X}}_2, \ldots, \tilde{\mathbf{X}}_{N-1}]^T$$

in which matrices $\mathbf{X}_n$ and $\tilde{\mathbf{X}}_n$ are, respectively, defined as

$$\mathbf{X}_n = [x(n,0,0), \ldots, x(n,k,q), \ldots, x(n,K-1,Q-1)]^T$$

with $x(n,k,q) = x(n-q)|x(n-q)|^{2k}$ being the nonlinear kernel for the MP model, and

$$\tilde{\mathbf{X}}_n = [x(n,0,0,0), \ldots, x(n,q,m,l), \ldots, x(n,Q+L-1,Q+L-1,Q+L-1)]^T$$

with $x(n,q,m,l) = x(n-q)x(n-m)x^*(n-l)$.

The solution to (24), i.e., the parameter estimation, can be derived by applying the least square (LS) algorithm as [23], [25]

$$\hat{\mathbf{\Omega}} = [\hat{\mathbf{W}}, \hat{\mathbf{\Theta}}] = (\mathbf{X}^H\mathbf{X})^{-1}\mathbf{X}^H\mathbf{r}_{\mathrm{LNA}} \tag{25}$$

in which $\mathbf{X}^H$ indicates the conjugate transpose of a complex matrix $\mathbf{X}$.

Therefore, the digital canceling signal can now be reconstructed from the BB signal $x[n]$ as

$$c_2[n] = \sum_{k\in\mathcal{K}}\sum_{p\in\mathcal{P}} \hat{\omega}_{kq}x[n-p]|x[n-p]|^{2k} + \sum_{q\in\mathcal{Q}}\sum_{m\in\mathcal{M}}\sum_{l\in\mathcal{L}} \hat{\theta}_{qml}x[n-q]x[n-m]x^*[n-l] \tag{26}$$

which includes the multipath SI channel, the transmitter nonlinearity, and the receiver nonlinearity.

3) Analog Multipath Canceling Signal Conversion: By feeding $c_2[n]$ to the auxiliary transmitter, the analog canceling signal $c_2(t)$ is generated to subtract from the residual SI of the stage-I cancellation, i.e., $r_{C1}(t)$, following conventional designs [8], [9]. As the canceling signal $c_2(t)$ closely approximates the residual SI $r_{C1}(t)$ in amplitude but with 180° in phase, the residual SI is significantly mitigated after subtraction within the power, yielding a residual signal

$$r_{\mathrm{C2}}(t) = r_{\mathrm{LNA}}(t) - c_2(t) \tag{27}$$

which closely approximates zero, given the model parameters ω_{kq} and θ_{qml} being accurately estimated by (25).

IV. Simulation and Experimental Results

A. Simulation Condition and Results

During the simulations, we consider the multipath coupling channel between the transmit and receive chains has power profiles of −20, −60, −70, and −75 dB for delays of zero, one, two, and four samples, respectively, which is modified from [21], [22] to fit better to full-duplex transceiver scenarios.

TABLE I
System-Level Parameters of the Considered Full-Duplex Transceiver

Simulation Parameter	Value
Signal bandwidth	20 MHz
Transmission power	−10dBm ~ +30dBm
SNR of transmitters 1&2	60 dB
Antenna isolation	20 dB
Receiver noise floor	−97 dBm
Cascaded OIP3 of transmitter	+37 dBm
Cascaded IIP3 of receiver	−17 dBm

The −20-dB attenuation with zero delay results from either the 20-dB circulator isolation or antenna separation corresponding to a distance of roughly 20 cm between the transmit and receive antennas [20].

For transmitter nonlinearity simulation, the MP model in [15] is used here with coefficients being

$$a_{10} = 1.0513 + 0.0904j \quad a_{30} = -0.0542 - 0.2900j$$
$$a_{50} = -0.9657 - 0.7028j \quad a_{11} = -0.0680 - 0.0023j$$
$$a_{31} = 0.2234 + 0.2317j \quad a_{51} = -2451 - 0.3735j$$
$$a_{12} = 0.0289 - 0.0054j \quad a_{32} = -0.0621 - 0.0932j$$
$$a_{52} = 0.1229 + 0.1508j$$

while for receiver nonlinearity simulation, the memoryless model nonlinear model is used with coefficients being

$$b_1 = 1.0108 + 0.0858j$$
$$b_3 = 0.0879 - 0.1583j$$
$$b_5 = -1.0992 - 0.8891j.$$

To illustrate the relative strengths of the different components of the SI signal at different cancellation stages, the corresponding power levels are calculated with typical component parameters listed in Table I for a specified transmission power range from −10 to 30 dBm. Note that the LNA and the VGA in the receive chain are assumed to be capable of ideally amplifying the received signal at the ADC input to the desired voltage range of the ADC. Thus, the gains of the LNA and the VGA are not considered in the calculations without loss of generality.

As shown in Fig. 3, power levels of the transmitter nonlinearity and noise within the received SI signal are higher than the receiver noise floor when transmission power exceeds 5 dBm and thus needs to be considered and suppressed in the analog domain to avoid raising the receiver noise floor. For stage-I analog cancellation, the cancellation capability in the simulation is roughly 40 dB, which is limited to this value due to the presence of the space multipath components (40 dB below the main SI component). After analog cancellation in this stage, both the transmitter nonlinearity and noise are suppressed along with the SI signal. This result is consistent with other RF-tapping approaches in [4], [5], [9], and [10], because these designs share the same idea in essence, except

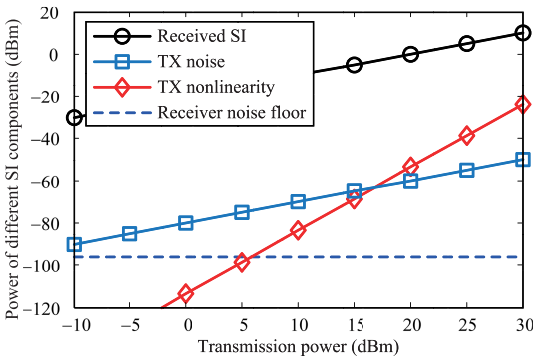

Fig. 3. Power levels of different signal components at the input of the receiver analog front-end (without analog SI cancellation).

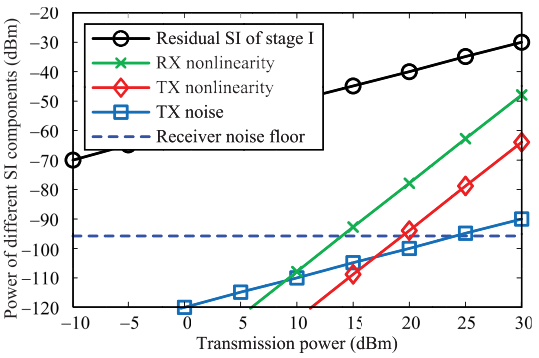

Fig. 4. Power levels of different signal components after stage-I analog cancellation.

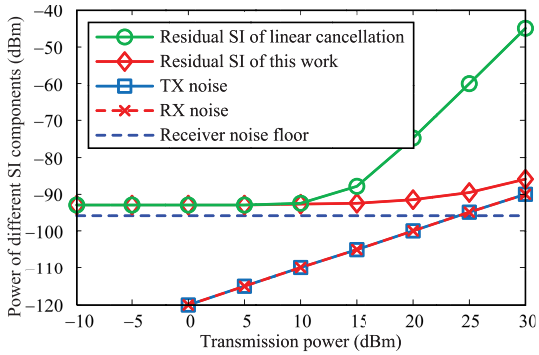

Fig. 5. Power levels of different signal components after stage-II analog cancellation.

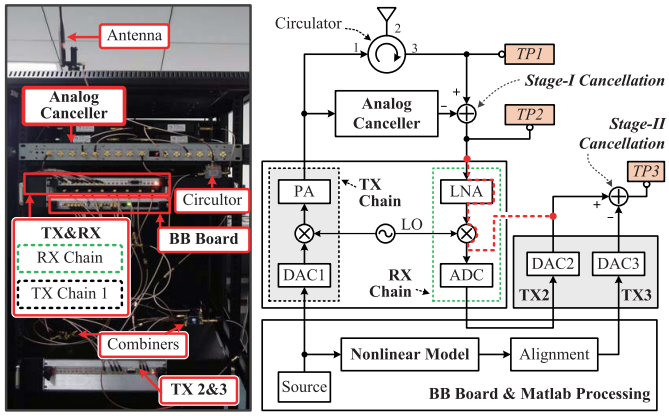

Fig. 6. Photograph and the block diagram of the experimental setup for the proposed two-stage analog cancellation performance verifications.

with structures of different complexities and accuracies to provide different cancellation capabilities. As shown in Fig. 3, the power levels of the residual SI after the proposed stage-I cancellation, the transmitter nonlinearity, and the transmitter noise are all attenuated by an amount of 40 dB.

The residual SI signal after stage-I analog cancellation enters the receive chain through some imperfect RF components, i.e., the LNA, the mixer, and the VGA. However, even after the stage-I analog cancellation, this residual SI is still 67 dB above the receiver noise floor for the case with transmission power being 30 dBm. By further considering the fact that the residual SI is distorted by these imperfect RF components, extra nonlinearity will be introduced. As shown in Fig. 4, the power level of the receiver nonlinearity of the residual SI signal also becomes observable when the transmission power exceeds 14 dBm.

To account for the joint effect of the multipath SI channel, the transmitter nonlinearity, and the receiver nonlinearity, we use the proposed nonlinear model in (23) instead of the linear model used in [9] in the stage-II analog cancellation for further SI mitigation. As a result, the residual multipath SI signal and its associated transmitter nonlinearity and receiver nonlinearity are all effectively suppressed to close to the receiver noise floor as shown in Fig. 5. Whereas the linear modeling approach in [9] mitigates only the linear component of the residual SI signal and provides poor cancellation capability when transmission power exceeds 10 dBm. Note that the small gap between the residual SI after stage-II analog cancellation and the receiver noise floor for transmission power below +25 dBm is caused by the modeling and cancellation process of this stage (the modeling and cancellation process is considered to have a 3-dB SNR loss on the processed signal in a more realistic way). Also note that when transmission power exceeds 25 dBm, the power of the residual SI slightly increases and raises the receiver noise floor. This is caused by the increase in the inherent noises from the two incoherent transmitters, which are by definition noises and are difficult to mitigate. Therefore, for high-power applications, larger antenna isolation and/or RF-tapping analog cancellation with higher cancellation capability will be required to ensure the BB-tapping analog cancellation functions properly.

B. Experimental Setup and Results

To verify the effectiveness of the two-stage analog SI cancellation architecture and evaluate the cancellation capability of each cancellation stage, a testbed is designed as shown in Fig. 6, where a photograph and a block diagram of the setup are illustrated. The BB board (labeled BB) provides the physical interfaces for the transmitter (labeled TX) and the receiver (labeled RX) of the full-duplex radio, as well as a USB cable to download/upload data from/to a computer running the MATLAB software. Within in the TX chain,

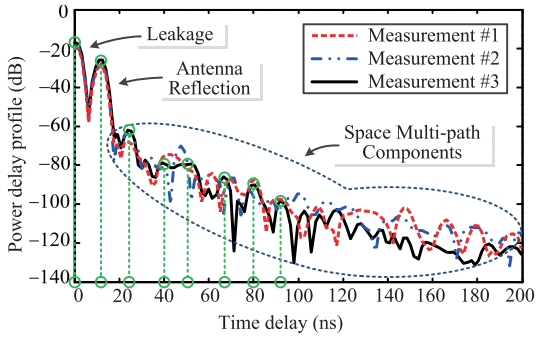

Fig. 7. Power delay profiles of the SI channel measured at different locations.

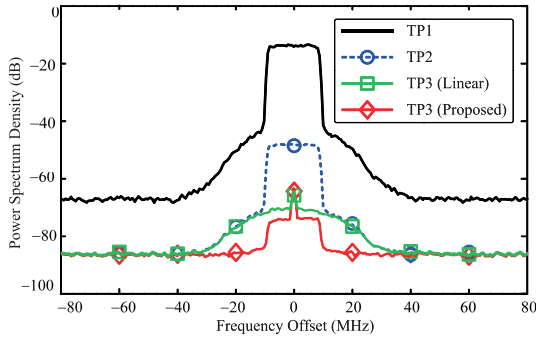

Fig. 8. Spectra of the 20-MHz signals at the three test points of the testbed at 17 dBm transmission power level.

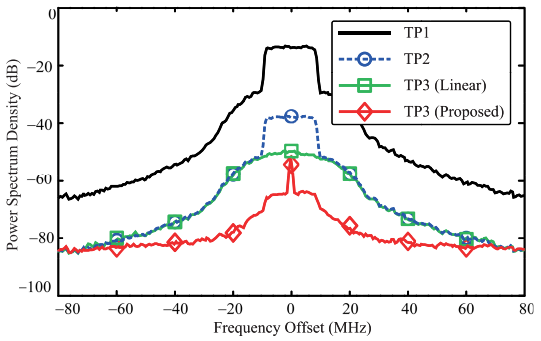

Fig. 9. Spectra of the 20-MHz signals at the three test points of the testbed at 27 dBm transmission power level.

a 1-W wideband amplifier (12-dB gain and 35-dB OIP3 at 2.35 GHz) is used to drive the transmitted signal to a maximum power level of 27 dBm to clearly demonstrate the nonlinear distortion. The transmitter TX and the receiver RX are then connected by a circulator with approximately 20-dB isolation, i.e., the direct leakage is approximately 20 dB lower than the transmit signal.

For stage-I analog cancellation, an analog canceller is designed following the RF-tapping approaches [4], [9], which couples the RF transmitted signal and passes it through two parallel reconstruction circuits for canceling signal generation. As illustrated in Fig. 2, each circuit is mainly composed of a phase shifter (PE44820, from Peregrine Semiconductor), a variable attenuator (EVA-3000+, from Mini-Circuits), and a field-programmable gate array chip that runs the gradient-based tuning algorithm for phase and attenuation adjustments and adaptations as introduced in Section III.

The experiments are performed at 2.4-GHz frequency band with 20 MHz signal bandwidth, in the center of a room ($14 \times 11 \times 3.3$ m^3). The power delay profiles of the indoor SI channel are measured with the antenna being place at 0.7, 1.7, and 2.4 m heights, respectively. As shown in Fig. 7, the leakage and the antenna reflection components are approximately 42 dB stronger than the space multipath components. In the multipath SI channel modeling process, to reconstruct a wide range of multipath components, an FIR filter with order being $L = 32$ is selected in (22), which is capable of characterizing a maximum path delay of 104 ns (for an ADC sampling rate of 307.2 MS/s). To reduce the number of the coefficients for the joint nonlinear model in (23), we select only some of the delays for implementation, as shown by the dashed lines in Fig. 7 where only the paths of delays being 0, 10, 22, 40, 46, 63, 80, and 93 ns are selected to reconstruct the space multipath components (corresponding to delays of 0, 3, 7, 12, 14, 20, 25, and 29 samples, respectively).

After stage-I analog cancellation, the residual SI $r_{\mathrm{LNA}}(t)$ is captured by the RX chain, digitized, and stored as $r_{\mathrm{LNA}}[n]$ for the propagation channel modeling (both the transmitter nonlinearity and the receiver nonlinearity are included). As presented in Section III-B, the stored residual SI signal $r_{\mathrm{LNA}}[n]$ and the source signal $x[n]$ are synchronized and organized in a matrix form as shown in (24) to extract the coefficients $\hat{\mathbf{\Omega}}$ through the LS algorithm as shown in (25). Subsequently, the extracted coefficients $\hat{\mathbf{\Omega}}$ are used to generate a digital canceling signal $c_2[n]$ through the proposed nonlinear model in (23). $c_2[n]$ is then transmitted through another transmitter (labeled TX3) to generate an analog canceling signal of low carrier frequency $c_2(t)$. Due to the limit of our testbed, the physical chain between the two power combiners (including the LNA, the mixer, and associated circuits illustrated as the red dashed line in Fig. 6) is not available at the current stage. In this experiment, without loss of generality, we combine the current RX chain and an extra transmitter (labeled TX2) to regenerate the residual SI with low carrier frequency $r_{\mathrm{LNA}}(t)$ from the stored digital SI $r_{\mathrm{LNA}}[n]$ to replace the physical chain. After fine alignment in digital domain, the canceling signal $c_2(t)$ would closely match the regenerated residual signal $r_{\mathrm{LNA}}(t)$ in amplitude but with 180° phase shift. By redirecting these two signals to the power combiner, the residual signal could be mitigated.

To evaluate the RF cancellation performances of the two analog cancellation stages, the spectra of signals at the three test points (labeled TP1, TP2, and TP3 in Fig. 6) are measured, corresponding to the signals before analog cancellation, after stage-I cancellation, and after stage-II cancellation, respectively. In stage-II cancellation, the linear cancellation approach in [9] is also implemented and measured for comparison.

The RF cancellation performances for a 20-MHz long-term evolution (LTE) signal are shown in Figs. 8 and 9 for transmission power levels of 17 and 27 dBm, respectively. It can be seen that the stage-I cancellation attenuates the power of the SI signal by almost 37 dB for both cases, due to fact that the adopted RF-tapping approach in this cancellation stage is

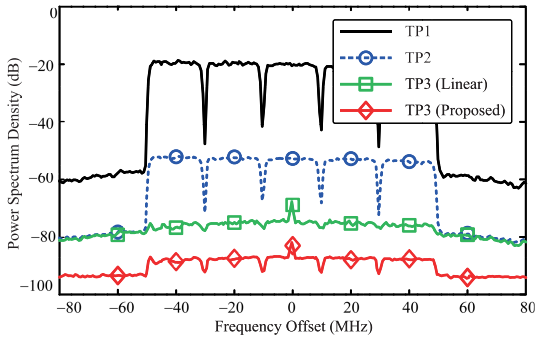

Fig. 10. Spectra of the 100-MHz signals at the three test points of the testbed at 17-dBm transmission power level.

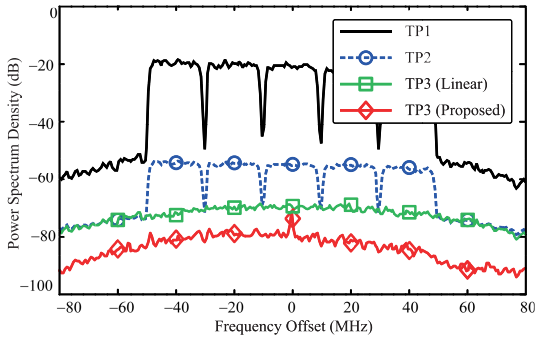

Fig. 11. Spectra of the 100-MHz signals at the three test points of the testbed at 27-dBm transmission power level.

capable of attenuating the transmitter nonlinearity and noise along with the SI. The stage-II cancellation with the proposed nonlinear modeling attenuates the power of the multipath SI signal by another 29 dB for both transmission power levels. As a comparison, the stage-II cancellation with linear modeling method [9] attenuates the power of the multipath SI signal by 20 and 15 dB for transmission power levels of 17 and 27 dBm, respectively. The dramatic drop in the cancellation performances is due to the increased nonlinear distortion within SI caused by the joint effect of the transmitter nonlinearity and the receiver nonlinearity, which are not included in the linear modeling method. This result is consistent with simulation results in Figs. 4 and 5.

The RF cancellation performances for a 100-MHz LTE-advanced signal are shown in Figs. 10 and 11 for transmission power levels of 17 and 27 dBm, respectively. It can be seen that the stage-I cancellation attenuates the power of the SI signal by approximately 37 dB for both cases, which is only 2 dB lower than the case with 20 MHz bandwidth. The stage-II cancellation with the proposed nonlinear modeling attenuates the power of the multipath SI signal by another 29 dB for both transmission power levels. Whereas the stage-II cancellation with linear modeling approach [9] attenuates only the power of the multipath signal by 21 and 10 dB for transmission power levels of 17 and 27 dBm, respectively. Compared with 20-MHz LTE signal, the LTE-advanced signal of 100-MHz bandwidth demonstrates more severe nonlinear distortion caused by the transmitter and the receiver. As the transmission power increases, the distortion becomes more obvious, resulting in an increase of the receiver nonlinear distortion and hence a cancellation performance degradation for linear modeling approaches [8], [9].

Therefore, the two-stage analog cancellation with nonlinear modeling can provide an overall analog cancellation of up to 66 dB, which is roughly 13 dB higher than the RF-tapping canceller in [26]. Such high cancellation on the SI signal could effectively prevent the ADC of the receive chain from being saturated. After this analog cancellation, the desired signal from a remote user could now enter the local receive chain for further processing.

V. Conclusion

A full-duplex transceiver of a novel analog cancellation architecture is proposed for the prevailing full-duplex wireless communications, by exploiting the structures of the conventional RF-tapping [5] and digital-tapping [8] approaches, and incorporating their advantages. Particularly, the proposed architecture uses a nonlinear model to characterize the joint effect of the multipath SI channel, the transmitter nonlinearity, and the receiver nonlinearity to yield a reconstruction of the multipath SI signal with improved accuracy. The effectiveness of the analog cancellation method is validated by a self-designed testbed with 20-MHz and 100-MHz LTE signals. This architecture provides an alternative solution to suppress the strong SI of wide range of multipath components as well as the nonlinearities of the transmitter and the receiver.

In future work, we plan to investigate the effect of this proposed two-stage analog SI cancellation scheme on the demodulation of the desired signal from a remote user. As high-power transmission will inevitably place stringent requirements on the BB-tapping structure, we also plan to investigate antenna-domain and RF-tapping approaches of higher cancellation capabilities to work with the BB-tapping approach to provide satisfactory SI cancellation even in high-power applications.

References

[1] E. Ahmed and A. M. Eltawil, "All-digital self-interference cancellation technique for full-duplex systems," *IEEE Trans. Wireless Commun.*, vol. 14, no. 7, pp. 3519–3532, Jul. 2015.

[2] A. Sabharwal, P. Schniter, D. Guo, D. W. Bliss, S. Rangarajan, and R. Wichman, "In-band full-duplex wireless: Challenges and opportunities," *IEEE J. Sel. Areas Commun.*, vol. 32, no. 9, pp. 1637–1652, Sep. 2014.

[3] C. Li, B. Xia, S. Shao, Z. Chen, and Y. Tang, "Multi-User scheduling of the full-duplex enabled two-way relay systems," *IEEE Trans. Wireless Commun.*, vol. 16, no. 2, pp. 1094–1106, Dec. 2016.

[4] M. Jain *et al.*, "Practical, real-time, full duplex wireless," in *Proc. Annu. Int. Conf. Mobile Comput. Netw.*, Las Vegas, NV, USA, Sep. 2011, pp. 301–312.

[5] D. Bharadia, E. McMilin, and S. Katti, "Full duplex radios," in *Proc. ACM Special Interest Group Data Commun. (SIGCOMM)*, Hong Kong, Aug. 2013, pp. 375–386.

[6] B. P. Day, A. R. Margetts, D. W. Bliss, and P. Schniter, "Full-duplex MIMO relaying: Achievable rates under limited dynamic range," *IEEE J. Sel. Areas Commun.*, vol. 30, no. 8, pp. 1541–1553, Sep. 2012.

[7] B. P. Day, A. R. Margetts, D. W. Bliss, and P. Schniter, "Full-duplex bidirectional MIMO: Achievable rates under limited dynamic range," *IEEE Trans. Signal Process.*, vol. 60, no. 7, pp. 3702–3713, Jul. 2012.

[8] M. Duarte, C. Dick, and A. Sabharwal, "Experiment-driven characterization of full-duplex wireless systems," *IEEE Trans. Wireless Commun.*, vol. 11, no. 12, pp. 4296–4307, Dec. 2012.

[9] X. Quan, Y. Liu, W. Pan, Y. Tang, and K. Kang, "A two-stage analog cancellation architecture for self-interference suppression in full-duplex communciations," in *IEEE MTT-S Int. Microw. Symp. Dig.*, Jun. 2017, pp. 1–4.

[10] K. E. Kolodziej, J. G. McMichael, and B. T. Perry, "Multitap RF canceller for in-band full-duplex wireless communications," *IEEE Trans. Wireless Commun.*, vol. 15, no. 6, pp. 4321–4334, Jun. 2016.
[11] A. Raghavan, E. Gebara, E. M. Tentzeris, and J. Laskar, "Analysis and design of an interference canceller for collocated radios," *IEEE Trans. Microw. Theory Techn.*, vol. 53, no. 11, pp. 3498–3508, Nov. 2005.
[12] Y. Liu, X. Quan, S. Shao, and Y. Tang, "Digital predistortion architecture with reduced ADC dynamic range," *Electron. Lett.*, vol. 52, no. 6, pp. 435–437, Mar. 2016.
[13] D. Korpi, L. Anttila, V. Syrjälä, and M. Valkama, "Widely linear digital self-interference cancellation in direct-conversion full-duplex transceiver," *IEEE J. Sel. Areas Commun.*, vol. 32, no. 9, pp. 1674–1687, Sep. 2014.
[14] R. Raich and G. T. Zhou, "Orthogonal polynomials for complex Gaussian processes," *IEEE Trans. Signal Process.*, vol. 52, no. 10, pp. 2788–2797, Oct. 2004.
[15] L. Ding *et al.*, "A robust digital baseband predistorter constructed using memory polynomials," *IEEE Trans. Commun.*, vol. 52, no. 1, pp. 159–165, Jan. 2004.
[16] D. Korpi, T. Riihonen, V. Syrjälä, L. Anttila, M. Valkama, and R. Wichman, "Full-duplex transceiver system calculations: Analysis of ADC and linearity challenges," *IEEE Trans. Wireless Commun.*, vol. 13, no. 17, pp. 3821–3836, Jul. 2014.
[17] H. Suzuki, T. V. A. Tran, I. B. Collings, G. Daniels, and M. Hedley, "Transmitter noise effect on the performance of a MIMO-OFDM hardware implementation achieving improved coverage," *IEEE J. Sel. Areas Commun.*, vol. 26, no. 6, pp. 867–876, Aug. 2008.
[18] W. Namgoong, "Modeling and analysis of nonlinearities and mismatches in AC-coupled direct-conversion receiver," *IEEE Trans. Wireless Commun.*, vol. 4, no. 1, pp. 163–173, Jan. 2005.
[19] X. Wu, Y. Shen, Y. Tang, and G. Hz, "The power delay profile of the singleantenna full-duplex self-interference channel in indoor environments at 2.6 GHz," *IEEE Antennas Wireless Propag. Lett.*, vol. 13, no. 1, pp. 1561–1564, Jan. 2014.
[20] A. Sahai, G. Patel, and A. Sabharwal, "Pushing the limits of full-duplex: Design and real-time implementation," Rice Univ., Houston, TX, USA, Tech. Rep. TREE1104, 2011.
[21] V. Syrjala, M. Valkama, L. Anttila, T. Riihonen, and D. Korpi, "Analysis of oscillator phase-noise effects on self-interference cancellation in full-duplex OFDM radio transceivers," *IEEE Trans. Wireless Commun.*, vol. 13, no. 12, pp. 2977–2990, Jun. 2014.
[22] X. Quan, Y. Liu, S. Shao, C. Huang, and Y. Yang, "Impacts of phase noise on digital self-interference cancellation in full-duplex communications," *IEEE Trans. Signal Process.*, vol. 65, no. 7, pp. 1881–1894, Apr. 2014.
[23] W. Chen, S. Zhang, Y. J. Liu, F. M. Ghannouchi, Z. Feng, and Y. Liu, "Efficient pruning technique of memory polynomial models suitable for PA behavioral modeling and digital predistortion," *IEEE Trans. Microw. Theory Techn.*, vol. 62, no. 10, pp. 2290–2299, Oct. 2014.
[24] Y. Liu, W. Pan, S. Shao, and Y. Tang, "A general digital predistortion architecture using constrained feedback bandwidth for wideband power amplifiers," *IEEE Trans. Microw. Theory Techn.*, vol. 63, no. 5, pp. 1544–1555, May 2015.
[25] L. Guan and A. Zhu, "Green communications," *IEEE Microw. Mag.*, vol. 15, no. 7, pp. 84–99, Dec. 2014.
[26] J. Tamminen *et al.*, "Digitally-controlled RF self-interference canceller for full-duplex radios," in *Proc. Eur. Signal Process. Conf.*, Aug. 2016, pp. 783–787.

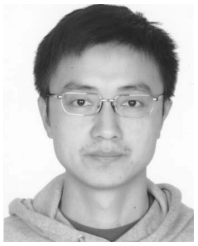

Ying Liu (S'13–M'16) received the B.E. and M.S. degrees in communication engineering and Ph.D. degree in communication and information system from the University of Electronic Science and Technology of China (UESTC), Chengdu, China, in 2008, 2011, and 2016 respectively.

He was a Visiting Scholar with the Department of Electrical and Computer Engineering, The Ohio State University, Columbus, OH, USA. He is currently a Lecturer with the National Key Laboratory of Science and Technology on Communications, UESTC, where he is also a Post-Doctoral Researcher with the School of Electronic Engineering. His current research interests include nonlinear modeling, digital predistortion, full-duplex wireless communications, and signal processing in wireless communications.

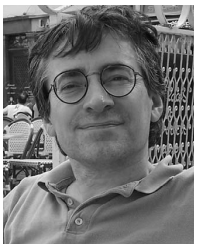

Patrick Roblin (M'85–SM'14) received the Maitrise de Physics degree from Louis Pasteur University, Strasbourg, France, in 1980, and the M.S. and D.Sc. degrees in electrical engineering from Washington University, St. Louis, MO, USA, in 1982 and 1984, respectively.

In 1984, he joined the Department of Electrical Engineering, The Ohio State University (OSU), Columbus, OH, USA, as an Assistant Professor, where he is currently a Professor. He is the lead author of the two textbooks *High-Speed Heterostructure and Devices* (Cambridge Univ. Press, 2002) and *Nonlinear RF Circuits and Nonlinear Vector Network Analyzers* (Cambridge Univ. Press, 2011). He is the Founder of the Non-Linear RF Research Laboratory, OSU. He has developed two educational RF/microwave laboratories and associated curriculum for training both undergraduate and graduate students. His current research interests include the measurement, modeling, design, and linearization of nonlinear RF devices and circuits such as oscillators, mixers, and power amplifiers.

Xin Quan (S'13) was born in Hebei, China, in 1988. She received the B.E. degree in communication engineering from Yanshan University, Qinhuangdao, China, in 2010, and the M.S. degree in communication and information system from the University of Electronic Science and Technology of China, Chengdu, China, in 2013, where she is currently pursuing the Ph.D. degree in communication and information system at the National Key Laboratory of Science and Technology on Communications.

She was a Visiting Scholar with the Department of Electrical and Computer Engineering, The Ohio State University, Columbus, OH, USA. Her current research interests include channel estimation, interference suppression, full duplex, and signal processing in wireless communications.

Wensheng Pan was born in Chongqing, China, in 1975. He received the B.E. and M.S degrees in communication engineering from the University of Science and Technology of China, Hefei, China, in 1998 and 2005, respectively. He is currently pursuing the Ph.D. degree at the Key Laboratory of Science and Technology on Communications, University of Electronic Science and Technology of China, Chengdu, China.

From 2005 to 2009, he served as a Manager with NtS-Technology Inc. His current research interests include power amplifier design, power amplifier linearization, digital predistortion, and crest factor reduction.

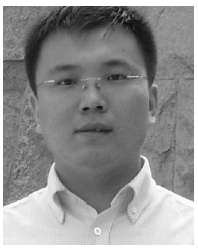

Shihai Shao (GS'05–M'10) was born in Liaoning, China, in 1980. He received the B.E. and Ph.D. degrees in communication and information system from the University of Electronic Science and Technology of China (UESTC), Chengdu, China, in 2003 and 2008, respectively.

Since 2008, he has been a Professor with the National Key Laboratory of Science and Technology on Communications, UESTC. His current research interests include full-duplex communications, signal processing in wireless communications, spread spectrum, and MIMO detection.

Youxi Tang was born in Henan, China, in 1964. He received the B.E. degree in radar engineering from the College of PLA Ordnance, Shijiazhuang, China, in 1985, and the M.S. and Ph.D. degrees in communications and information systems from the University of Electronic Science and Technology of China (UESTC), Chengdu, China, in1993 and 1997, respectively.

From 1998 to 2000, he was a Program Manager with the Huawei Technologies Company Ltd., Shanghai, China, where he was involved in IS-95 mobile communications and third-generation mobile communications. Since 2000, he has been a Professor with the National Key Laboratory of Science and Technology on Communications, UESTC. His current research interests include spread spectrum systems and wireless mobile systems with an emphasis on signal processing in communications.